10th March 2018

Triphasic Nature of Polymers of Intrinsic Microporosity (PIM-1 and PIM-PY) Induces Storage and Catalysis Effects in Hydrogen and Oxygen Reactivity at Electrode Surfaces

Dr. Elena Madrid [1], Dr. John P. Lowe [1], Dr. Kadhum J. Msayib [2], Prof. Neil B. McKeown [2], Dr. Qilei Song [3], Prof. Gary A. Attard [4], Prof. Tina Düren [5], and Prof. Frank Marken* [1]

[1] *Department of Chemistry, University of Bath, Claverton Down, Bath BA2 7AY, UK*

[2] *EAstChem School of Chemistry, University of Edinburgh, Joseph Black Building, David Brewster Rd., Edinburgh, Scotland EH9 3FJ, UK*

[3] *Department of Chemical Engineering, Imperial College London, London SW7 2AZ, UK*

[4] *Department of Physics, The Oliver Lodge Laboratory, University of Liverpool, Oxford Street, Liverpool L69 7ZE, UK*

[5] *Department of Chemical Engineering, Centre for Advanced Separation Engineering, University of Bath, Bath BA2 7AY, UK*

To be submitted to ChemElectroChem (2018 Special Anniversary Issue)

Proofs to F. Marken (f.marken@bath.ac.uk)

Abstract

Hydrogen oxidation and oxygen reduction are two crucial energy conversion reactions, which are shown to be both strongly affected by the presence of intrinsically microporous polymer coatings on electrodes. Polymers of intrinsic microporosity (PIMs) are known to possess extremely high internal surface area and ability to bind gases under dry conditions. It is shown here that both, hydrogen and oxygen gas binding into PIMs, also occurs under wet or "triphasic" conditions in aqueous electrolyte environments (when immersed in 0.01 M phosphate buffer at pH 7). For two known PIM materials (PIM-1 and PIM-PY) nanoparticles are formed by an anti-solvent precipitation protocol and then cast as a film onto platinum or glassy carbon electrodes. Voltammetry experiments reveal evidence for hydrogen and oxygen binding. Both, PIM-1 and PIM-PY, locally store hydrogen or oxygen gas at the electrode surface and thereby significantly affect electrocatalytic reactivity. The onset of oxygen reduction on glassy carbon is shifted by 0.15 V positive.

Graphical Abstract

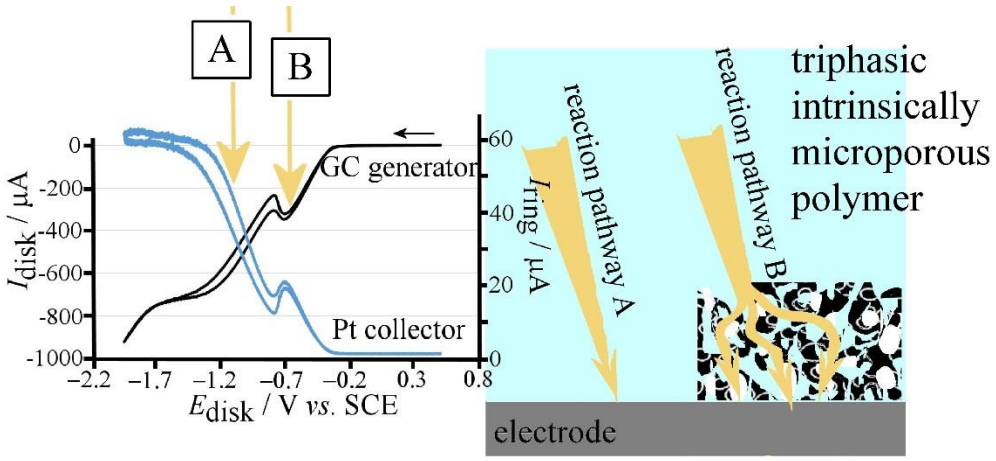

Due to their hydrophobic and molecularly rigid nature, intrinsically microporous polymers affect the conditions for gas | liquid electrolyte | solid electrode triphasic reactions.

Key words: electrocatalysis; voltammetry; modified electrode; diffusion; carbon dioxide

1. Introduction

Electrochemical processes based on hydrogen evolution/reduction and based on oxygen evolution/reduction are crucial in many area of energy technology such as fuel cell anodes and cathodes,[1,2] battery technology,[3] in artificial photosynthesis,[4] and in water electrolysis.[5] Materials that can catalyse or affect the electrocatalytic reactivity at interfaces are therefore of special importance, in particular when these materials offer additional benefits such as gas adsorption of (or) accumulation effects. Microporous materials are now widely studied and rapidly developing for example based on metal-organic frameworks,[6] covalent organic frameworks,[7] zeolites,[8] porous organic materials,[9] and molecularly designed carbons.[10] A particularly interesting class of new and versatile synthetic materials are the Polymers of Intrinsic Microporosity (PIMs).

PIMs have been developed as a novel class of highly molecularly rigid polymer systems with good solubility and therefore also good processability.[11,12] PIM-1 and PIM-PY (see Figure 1) both exhibit nitrogen adsorption isotherm or BET surface areas of ~750 m^2 g^{-1} were first synthesised by Budd et al.[13] and by Kricheldorf et al.,[14] respectively. These and related intrinsically microporous polymers have been proposed for a range of interesting applications including gas separation,[15] gas storage,[16] hydrogen storage,[17] sensing of gases,[18] reagent-less electrochemiluminescence,[19] and in electrochemical redox flow cell membranes with high selectivity.[20]

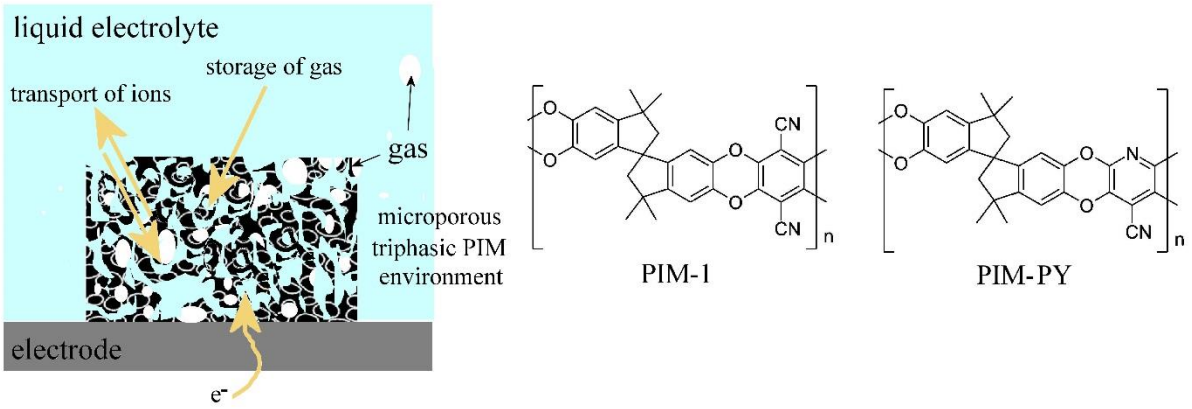

Figure 1. Scheme of triphasic electrode modification and molecular structures for PIM-1 and PIM-PY.

Only recently has the potential of PIMs in electrochemical processes been explored in more depth.[21] It was observed that ion conducting and semipermeable ion conducting properties are observed as a function of solution concentration and pH.[22,23] PIM materials that allow protonation also gave novel ionic diode (or rectification) effects,[24] and this was then suggested to lead to opportunities for example in novel desalination processes.[25] PIM materials were employed to stabilise nanoparticulate catalysts[26,27] and to affect the pathway of corrosion processes.[28] PIM-1 has been shown to produce electrochemiluminescence effects in aqueous media.[19] When gently carbonised, PIM materials have been demonstrated to retain their microporosity, whilst allowing electrical conductivity and supercapacity effects to be observed.[29,30] Noble metal nanoparticle catalysts were embedded into the carbonised PIM hosts[31,32] and shown to give encapsulated catalysts with altered reactivity. Intriguingly, the case of palladium nanoparticles encapsulated in carbonised PIM has been suggested to exhibit "triphasic" characteristics that affect electrocatalytic properties.[32] The term "triphasic" here denotes a material with solid, liquid, and gaseous content (Figure 1).

The structure of PIM-1 is sensitive to transformations both in the presence of solvents or alkaline reagents[33,34] and when exposed to UV radiation.[35] When formed into films and membranes, structural variations during thermal cross-linking have been noted.[36] In spite of this complexity, this intrinsically microporous polymer offers a wealth of new insights and may be considered a model system for the study of properties and applications of intrinsically microporous polymers in general. Particular emphasis in this report is on the triphasic nature of these materials.

Triphasic materials are of interest in modified electrodes and in electrocatalysis. The fundamental concept is based on the hydrophobicity of a part of the microporous structure causing entrapment of gas, presumably in very small bubbles or inclusions (see Figure 1). Water and aqueous electrolyte media penetrate readily into PIM-1 and PIM-PY films, but not all of the gas phase is replaced and therefore a triphasic system is formed with solid polymer, liquid electrolyte, and gas inclusions simultaneously present as a stable multi-phase system. However, at the scale of micropores (ca. 1 nm) the definition of the terms such as "phase" and "gas bubble" need to be re-considered as traditional phase boundaries may not be formed, even though a gas-like mobile state may be retained. Examples of triphasic systems are known for

metal-organic frameworks,[37] clays,[38] zeolites,[39] and porous carbons.[40] The presence of the liquid sometimes serves to enhance the gas binding ability of the microporous material.[41] Related hydrogen storage effects in porous organic hosts deposited onto platinum electrodes have also recently been noted to affect electrode processes.[42]

In this study we explore hydrogen gas adsorption within the microporous PIM-1 and PIM-PY *in situ* when deposited onto the surface of a platinum electrode and immersed into aqueous electrolyte solution. Both the hydrogen accumulation effects due to binding and the effects of hydrogen mobility are investigated for nanoparticulate films of PIM-1 and PIM-PY and contrasted to dense PIM film deposits. The effects of oxygen accumulation into PIM-1 and into PIM-PY are shown to affect the electrocatalytic formation of hydrogen peroxide at glassy carbon electrodes. Future applications are proposed in energy storage processes and in electrocatalytic processes involving gas intermediates for energy devices.

2. Experimental

2.1. Chemical Reagents

Polymer PIM-1 and PIM-PY were prepared following a literature procedure.[43] Chloroform, methanol and phosphoric acid (H_3PO_4 85%) and sodium hydroxide (NaOH 98%) were purchased from Sigma-Aldrich and used without further purification. Argon, oxygen, and hydrogen gases were purchased from BOC UK (Pureshield).

2.2. Instrumentation

An Autolab potentiostat system (PGSTAT12, EcoChemie, The Netherlands) was employed to control the electrochemical processes. Data were recorded using GPES software. A conventional three-electrode glass cell was used with a glassy carbon or platinum working electrode (both of 3 mm diameter), a KCl-saturated calomel electrode (SCE, Radiometer, Copenhagen) as the reference electrode, and a platinum wire as the counter electrode (Advent Materials UK). The experiments were performed under ambient conditions ($T = 20 \pm 2$ °C).

To ensure the working electrode was clean and the surface was reproducible, the electrode was polished using 0.3 μm particle size alumina powder on a wet polishing micro-cloth, followed by rinsing with copious amounts of ultrapure water. The platinum electrode was also electrochemically pre-treated with 50 consecutive potential cycles from -0.22 V vs. SCE to +1.1 V vs. SCE (scan rate 0.1 V s^{-1}) in aqueous 0.5 M H_2SO_4. The electrode was then rinsed with water, dried in a stream of argon, and used in further experiments.

A 10 mM concentration of phosphate buffer solution (PBS) of pH 7 was used as a background electrolyte solution for all experiments. The buffer was prepared using deionized water of resistivity 18 MΩ cm at 22 °C from a Thermo Fisher water purification system. The pH of the solution was adjusted to 7 using sodium hydroxide and confirmed using a glass pH probe (Jenway). A rotating ring-disk electrode system with a 5.5 mm disk of glassy carbon and a concentric 2 mm wide platinum ring (AFE6R2GCPT, Pine Research) was modified with PIM-1 or PIM-PY nanoparticles and used for the detection of hydrogen peroxide produced by oxygen reduction at the glassy carbon electrode surface.

2.3. Preparation of PIM-1 and PIM-PY Nanoparticle Modified Electrodes

PIM nanoparticles (PIM-1 or PIM-PY) were synthesized by using the anti-solvent re-precipitation method. PIM polymer dissolved in chloroform (2 mL with 1 mg mL^{-1} concentration) was added dropwise into 20 mL of methanol with vigorous stirring at room temperature. The mixture was stirred for 12 h and then centrifuged for 30 min at 5000 rpm. Excess methanol was removed to give 0.5 mL. Then the PIM nanoparticles were re-dispersed by ultrasonication[19] in methanol. A volume of 5 μL of this 4 mg mL^{-1} PIM nanoparticle dispersion was then deposited onto the working electrode and allowed to air-dry to give a 20 μg deposit.

3. Results and Discussion

3.1. Formation of PIM-1 and PIM-PY Nanoparticle Film Deposits

The intrinsically microporous polymers PIM-1 and PIMI-PY are both highly soluble/processible in chloroform (1 mg mL^{-1}) and easily cast into thin films or coatings. However, it is also possible to form nanoparticulate aggregates by precipitation in anti-solvent

(here in methanol). Nanoparticulate polymer aggregates with approximately 10-30 nm particle diameter are obtained by injecting the chloroform solution into agitated methanol (see Experimental). Figure 2 shows scanning electron microscopy (SEM) images of PIM-1 and PIM-PY nanoparticle aggregates.

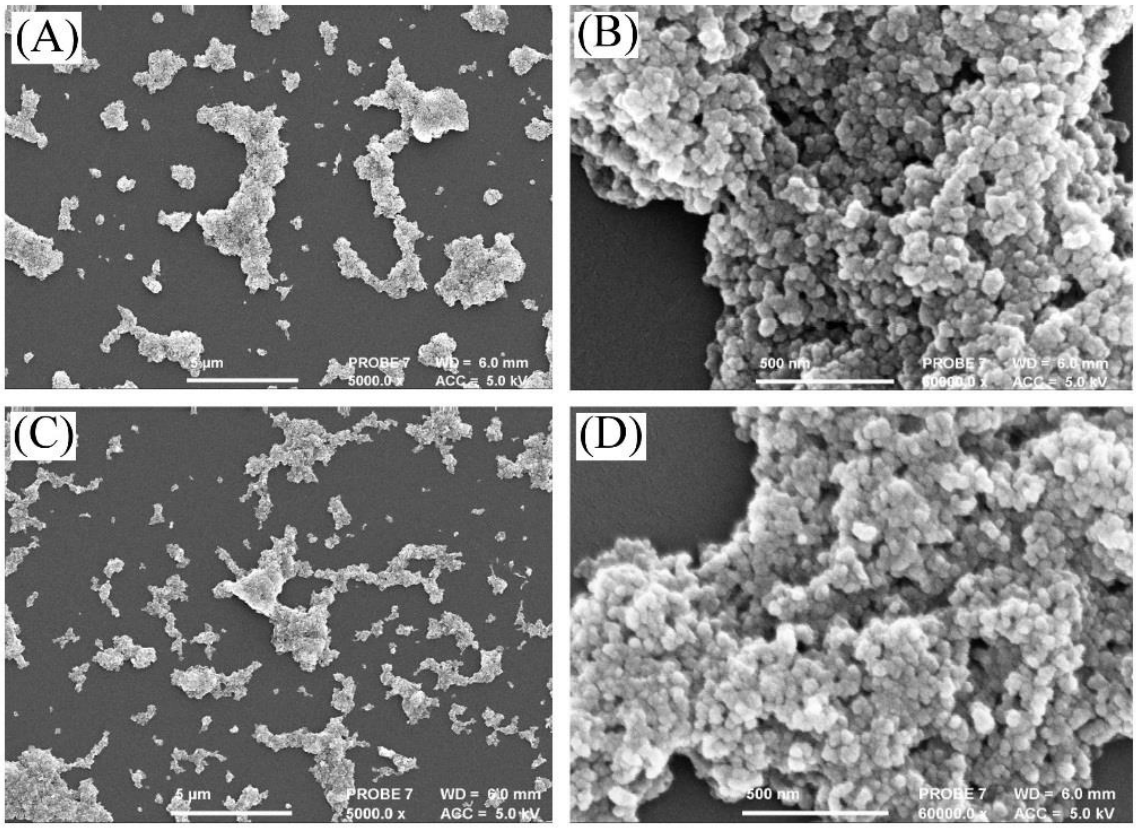

Figure 2. Scanning electron microscopy (SEM) images for (A,B) PIM-1 and (C,D) PIM-PY nanoparticles deposited onto a carbon surface.

3.2. Hydrogen Storage Effects at Electrode | PIM Interfaces

In voltammetry experiments at Pt working electrodes (in the given potential ranges) PIM polymers show no direct electrochemical activity. Figure 3A shows data for a deposit of PIM-1 nanoparticles (0.02 mg deposited onto a 3 mm diameter Pt working electrode) immersed in aqueous 0.01 M phosphate buffer. For the bare platinum (trace i) characteristic signals for platinum oxidation (broad anodic feature at 0.2 to 0.8 V vs. SCE) and back reduction (cathodic peak at 0.0 V vs. SCE) are observed. In the negative potential range two peaks denoted Process

1 and Process 2 are observed consistent (at least in first approximation[44]) with the formation of weakly and strongly adsorbed hydrogen, respectively (see equation 1 and 2).

$$\text{Process 1:} \quad H^+(aq) + e^-(Pt) \rightleftharpoons Pt\text{-}H(strong) \qquad (1)$$

$$\text{Process 2:} \quad H^+(aq) + e^-(Pt) \rightleftharpoons Pt\text{-}H(weak) \qquad (2)$$

In the presence of the PIM-1 nanoparticle coating all voltammetric signals appear suppressed (indicative of some platinum being inaccessible or coated to an extent of approximately 70%). All platinum peaks seem to develop cycle-by-cycle with the cathodic part of Process 1 appearing most prominently (Figure 3A). The reason for this could be linked to minor changes in the reaction environment such as small amounts of oxygen gas being trapped (*vide infra*), which is then visible as a peak close to the potential where Process 1 occurs.

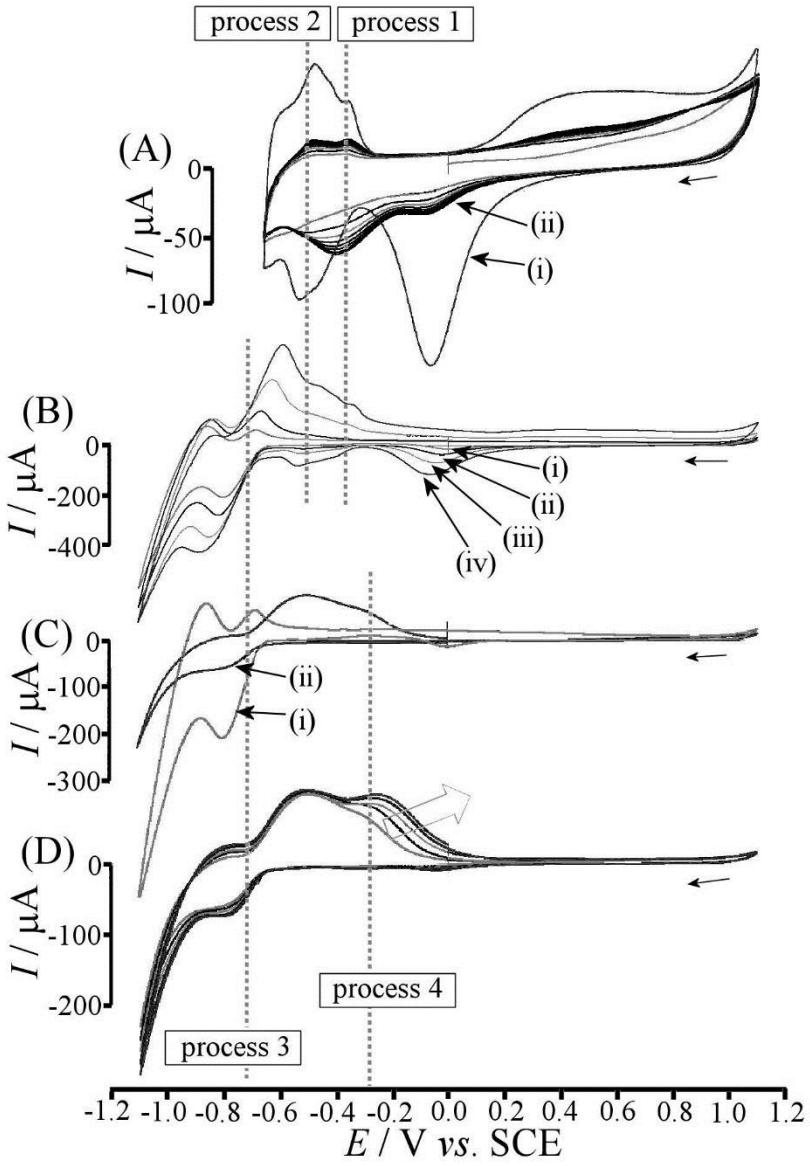

Figure 3. (A) Cyclic voltammograms (scan rate 50 mVs^{-1}) for a 3 mm diameter Pt disk electrode immersed in 0.01 M phosphate buffer pH 7.7 for (i) the bare electrode and (ii) a 20 μg PIM-1 nanoparticle deposit. (B) As before but for bare platinum scan rate (i) 50, (ii) 100, (iii) 250, (iv) 500 mVs^{-1} over an extended potential range. (C) As before for scan rate 50 mVs^{-1} and (i) bare platinum and (ii) 20 μg PIM-1 nanoparticle deposit. (D) As before but for five consecutive potential cycles.

When extending the potential window into the more negative range (Figure 3B), the bare platinum electrode shows the hydrogen evolution process as a well-defined reversible pair of peaks (reduction at -0.8 V vs. SCE and oxidation at approximately -0.6 V vs. SCE). This process is the hydrogen evolution reaction associated with the 10 mM pH 7 buffer system (see

equation 3). At more negative potentials of -1.0 V vs. SCE the bulk water reduction at locally more alkaline pH leads to further hydrogen evolution.

Process 3: $2\ H^+(aq) + 2\ e^- \rightleftharpoons H_2(g)$ (3)

Data in Figure 3C demonstrate the effect of the PIM-1 coating on the hydrogen evolution process. Although, the reduction process (Process 3) is somewhat suppressed (trace i, as expected due to partial electrode blocking with polymer) the anodic oxidation of hydrogen is actually increased (trace ii). When continuing to cycle the electrode over this potential range a new peak forms (denoted as Process 4 in Figure 3D) now associated with hydrogen oxidation from a reservoir of hydrogen in PIM-1 (see equation 4, *vide infra*). This process is believed to occur via a solution phase intermediate such as $H_2(aq)$ in close vicinity to the nanoparticulate polymer.

Process 4: $2\ H^+(aq) + 2\ e^- \rightleftharpoons H_2(aq) \rightleftharpoons H_2(PIM)$ (4)

Figure 4 demonstrates the effect of PIM-1 coating thickness on the voltammetric responses for proton reduction and hydrogen oxidation. By increasing the amount of PIM-1 nanoparticles on the platinum electrode surface most voltammetric features remain similar, but a new process (see Process 5 in Figure 4C) is indicative of yet another type of hydrogen oxidation process (equation 5). This process is believed to occur directly at the PIM-1|platinum interface (*vide infra*).

Process 5: $2\ H^+(aq) + 2\ e^- \rightleftharpoons H_2(PIM)$ (5)

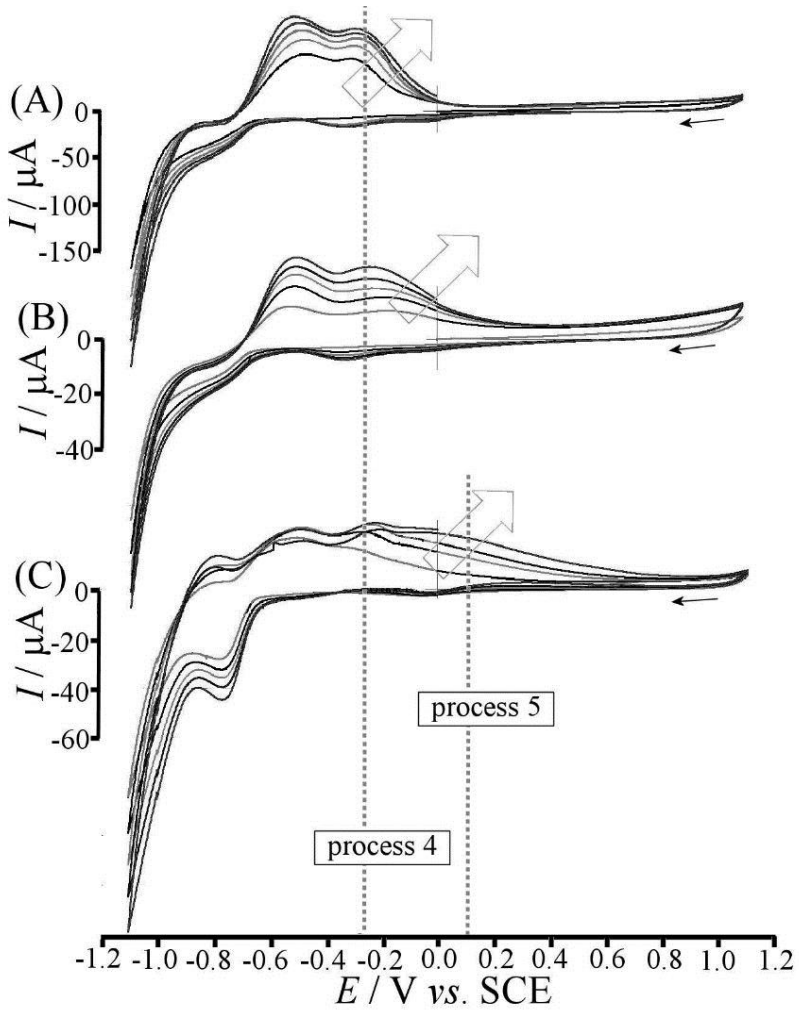

Figure 4. Cyclic voltammograms (scan rate 0.1 Vs^{-1}; five consecutive potential cycles) for a 3 mm diameter Pt disk electrode with (A) 20, (B) 40, (C) 60 µg PIM-1 nanoparticle deposits immersed in 0.01 M phosphate buffer pH 7.

The effect of the PIM-1 nanoparticle film thickness appears to be subtle, but it may be concluded that Process 5 is more obvious with a higher loading of PIM-1. Data in Figure 5A contrast the behaviour of bare platinum, a nanoparticle film deposit of PIM-1, and a nanoparticle film deposit of PIM-PY. Both types of intrinsically microporous polymers show similar features with the peak for Process 4 (shifted slightly due to a higher scan rate/range) being prominent.

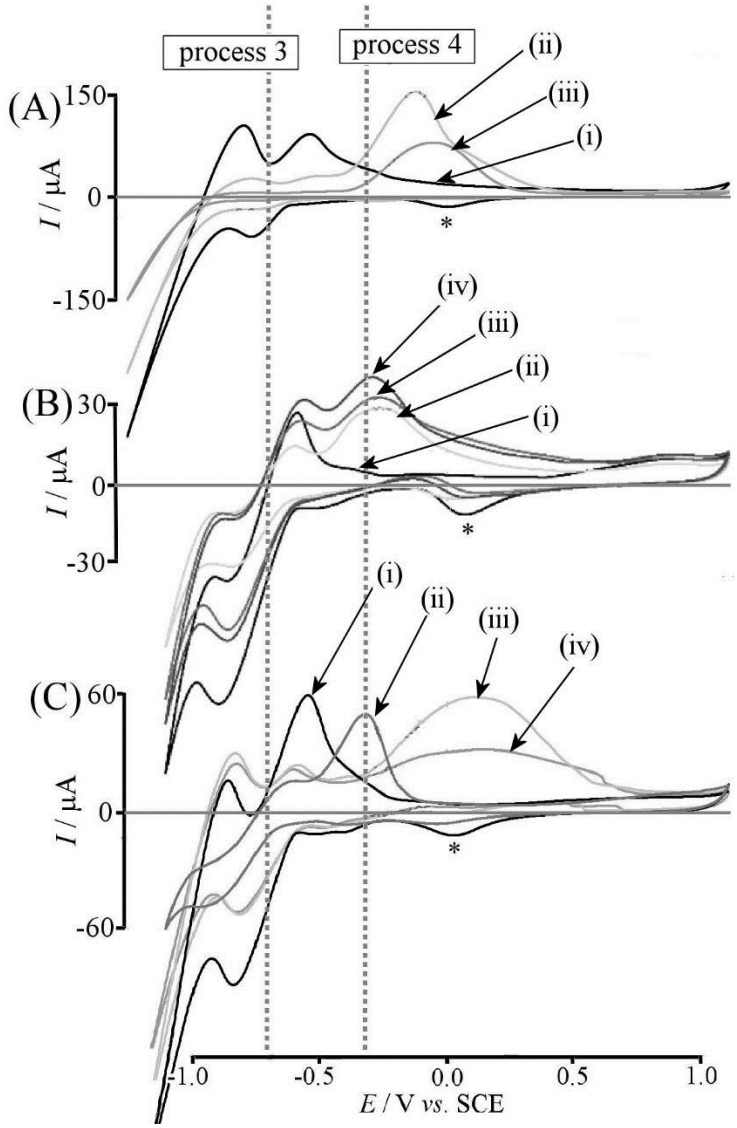

Figure 5. Cyclic voltammograms (scan rate 50 mV s^{-1}) for a 3 mm diameter platinum disk electrode immersed in 0.01 M phosphate buffer pH 7. (A) Comparison of (i) bare platinum, (ii) 20 μg PIM-1, and (iii) 20 μg PIM-PY nanoparticles. (B) Comparison of (i) bare platinum, (ii) 20 μg PIM-1, (iii) 40 μg PIM-1, and (iv) 60 μg PIM-1 nanoparticles. (C) Comparison of (i) bare platinum, (ii) 20 μg PIM-1 nanoparticles, (iii) 20 μg dense PIM-1 films, and (iv) 20 μg dense PIM-PY film. The * symbols indicates the cathodic peak for the platinum oxide to platinum surface reduction.

Data in Figure 5B demonstrate that an increase in the amount of PIM-1 nanoparticle deposit leads only to a small increase in the hydrogen oxidation response (process 4). A much bigger change is observed when instead of the nanoparticulate film a dense film of PIM-1 or PIM-PY is applied (Figure 5C). Experimentally, this approach is complicated by the possible lift-off of films from the electrode under gas evolution conditions, but for both types of polymers a clear shift in the anodic hydrogen oxidation response can be attributed to a change in mechanism

from that proposed in Process 4 to that proposed in Process 5. An asterisk (*) is used to indicate the platinum surface reaction associated with the cathodic conversion of platinum oxide to bare platinum.

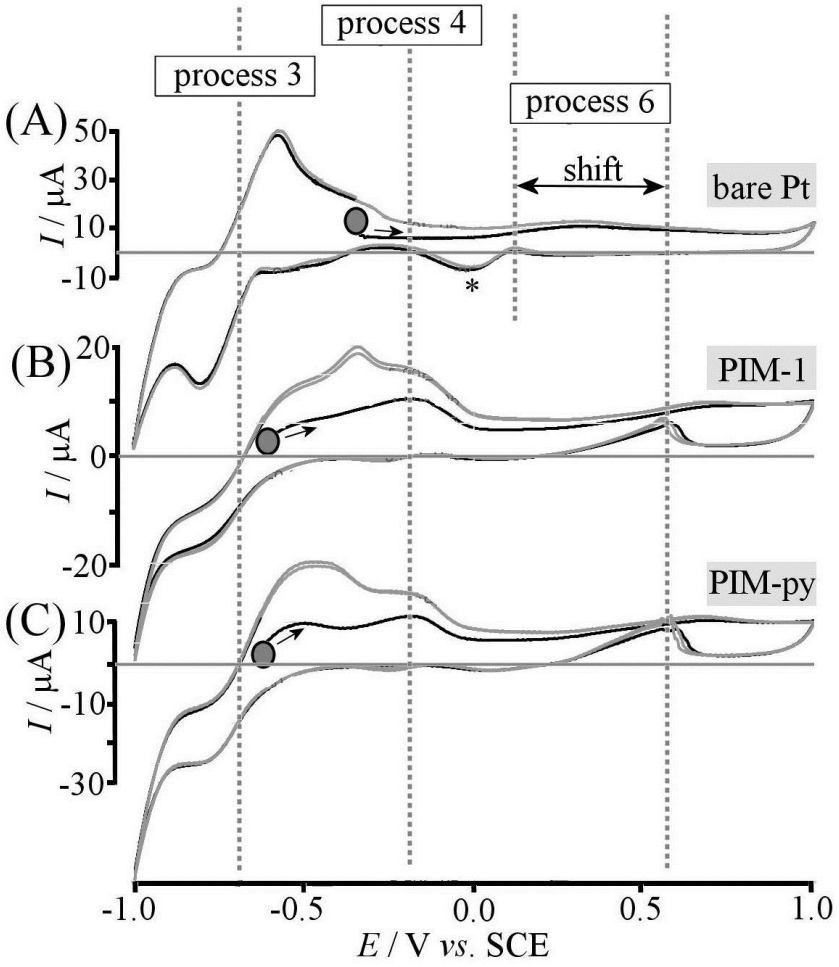

Figure 6. Cyclic voltammograms (scan rate 50 mVs^{-1}; three consecutive potential cycles) for (A) bare platinum, (B) 20 μg PIM-1 nanoparticle film, and (C) 20 μg PIM-PY nanoparticle film on a 3 mm diameter platinum electrode immersed into 0.01 M phosphate buffer pH 7 pre-saturated with hydrogen gas. Experiments were initiated at open circuit potential.

It is interesting to contrast the behaviour of hydrogen generated *in situ* at the platinum electrode surface with the behaviour when hydrogen is purged through the aqueous electrolyte solution. Figure 6A shows cyclic voltammograms for a bare platinum electrode in 0.01 M phosphate buffer. The proton reduction as formulated in Process 3 is observed as before. The voltammograms are shifted up in current due to the underlying hydrogen oxidation process. A new peak feature at 0.1 V vs. SCE (an anodic peak observed during the negative going potential

scan) signals the removal of the oxide layer from the platinum surface causing enhanced hydrogen oxidation. For both PIM-1 and PIM-PY nanoparticle deposits (see Figure 6B and 6C, respectively) the shape of voltammetric responses for Process 3 is modified in shape. Also, now a much clearer shift towards positive currents is observed for the feature indicated as Process 6, which is due to enhanced hydrogen oxidation in the presence of the polymer nanoparticles. The underlying process is linked to the effect of platinum oxide[45] on the hydrogen oxidation (equation 6). The anodic peak associated with enhanced hydrogen oxidation is shifted from 0.2 V to 0.6 V vs. SCE, which signals a substantial pH difference between solution phase and polymer-coated electrode surface. The shift of 0.4 V suggests a local pH more than 6 pH units more acidic, which must be associated with the ongoing hydrogen oxidation in the background. Therefore, conditions for electrocatalysis (here hydrogen oxidation) may be substantially different in the absence and in the presence of nanoparticulate coatings of polymer of intrinsic microporosity. These experiments also clearly signal the presence of a "reservoir" of hydrogen close to the platinum electrode surface (Process 4) in the first potential cycle when initiating the experiment under open circuit conditions.

Process 6: $PtO(s) + 2\,H^+(aq) + 2\,e^- \rightleftharpoons Pt(s) + H_2O$ (6a)

$H_2(aq) \rightleftharpoons + 2\,H^+(aq) + 2\,e^-$ (6b)

3.3. Oxygen Storage Effects at Electrode | PIM Interfaces

When performing experiments with PIM-1 and PIM-PY nanoparticle coatings on the surface of glassy carbon electrodes, no voltammetric response for hydrogen evolution and hydrogen oxidation are observed due to the absence of an effective catalyst. However, these types of electrodes are still able to bind gasses and this is demonstrated here for the oxygen reduction reaction at glassy carbon. Oxygen reduction is strongly dependent on the type of electrode material and catalysed by platinum surfaces and has often been studied in aqueous media and at glassy carbon electrode surfaces.[46,47]

Data in Figure 7A show the reduction of oxygen (i) at bare platinum, (ii) at PIM-1 nanoparticle coated platinum, and (iii) at PIM-PY nanoparticle coated platinum. In all three cases the underpotential responses for proton reduction (Process 1 and 2) are clearly observed. The reduction of oxygen in the absence of polymer occurs at less negative potential as a pre-wave (here probably caused by the pH local at the electrode surface). In the presence of polymer only one reduction peak is detected with a higher peak current. The pre-wave might be suppressed due to polymer restricting access of (the weak) buffer to the electrode surface. Figure 7B shows data for the polymer modified electrodes for a smaller potential window. In all cases the well-known four-electron reduction of oxygen on platinum is assumed as mechanism (Process 7, equation 7).

Process 7: $O_2(aq) + 4\,H^+(aq) + 4\,e^- \rightleftharpoons 2\,H_2O$ (7)

When investigating glassy carbon as substrate electrode material (Figure 7C), a much more dramatic change is observed. The reduction peak at -0.7 V vs. SCE is consistent with the two-electron reduction of oxygen to hydrogen peroxide (Process 8, equation 8). In the presence of either PIM-1 or PIM-PY nanoparticles a new pre-peak is observed which is likely to be associated with the reduction of oxygen "stored" in the intrinsically microporous polymer nanoparticles (Process 9, equation 9). The shift in the reduction peak of about 0.15 V towards more positive potential suggests a pathway that is significantly enhancing the oxygen reduction process.

Process 8: $O_2(aq) + 2\,H^+(aq) + 2\,e^- \rightleftharpoons H_2O_2$ (8)

Process 9: $O_2(PIM) + 2\,H^+(aq) + 2\,e^- \rightleftharpoons H_2O_2$ (9)

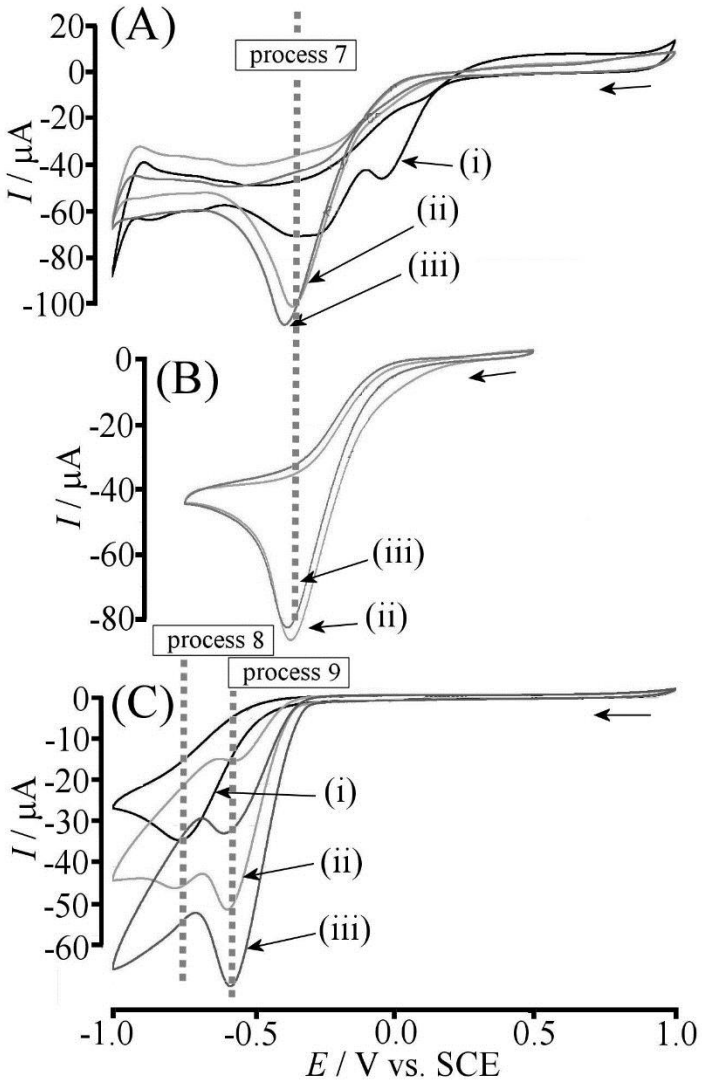

Figure 7. Cyclic voltammograms (scan rate 50 mVs^{-1}; 3 mm diameter electrodes) for the reduction of ambient oxygen in aqueous 0.01 M phosphate buffer solution at pH 7 for (A) (i) bare platinum, (ii) 20 µg nanoparticulate PIM-1, and (iii) 20 µg nanoparticulate PIM-PY, (B) (ii) 20 µg nanoparticulate PIM-1 on platinum and (iii) 20 µg nanoparticulate PIM-PY on platinum, (C) (i) bare glassy carbon, (ii) 20 µg nanoparticulate PIM-1 on glassy carbon, (iii) 20 µg nanoparticulate PIM-PY on glassy carbon.

In order to better understand this enhanced oxygen reduction reaction in the presence of the intrinsically microporous polymer rotating ring-disk experiments are performed. In this experiment hydrodynamic flow of liquid over the central glassy carbon disk is induced by rotation[48] and the out platinum ring electrode can be employed to detect products. Here, the potential applied to the platinum ring electrode is fixed at +0.3 V vs. SCE to detect hydrogen peroxide (see equation 8) as an anodic voltammetric response (oxidation of hydrogen peroxide to oxygen).

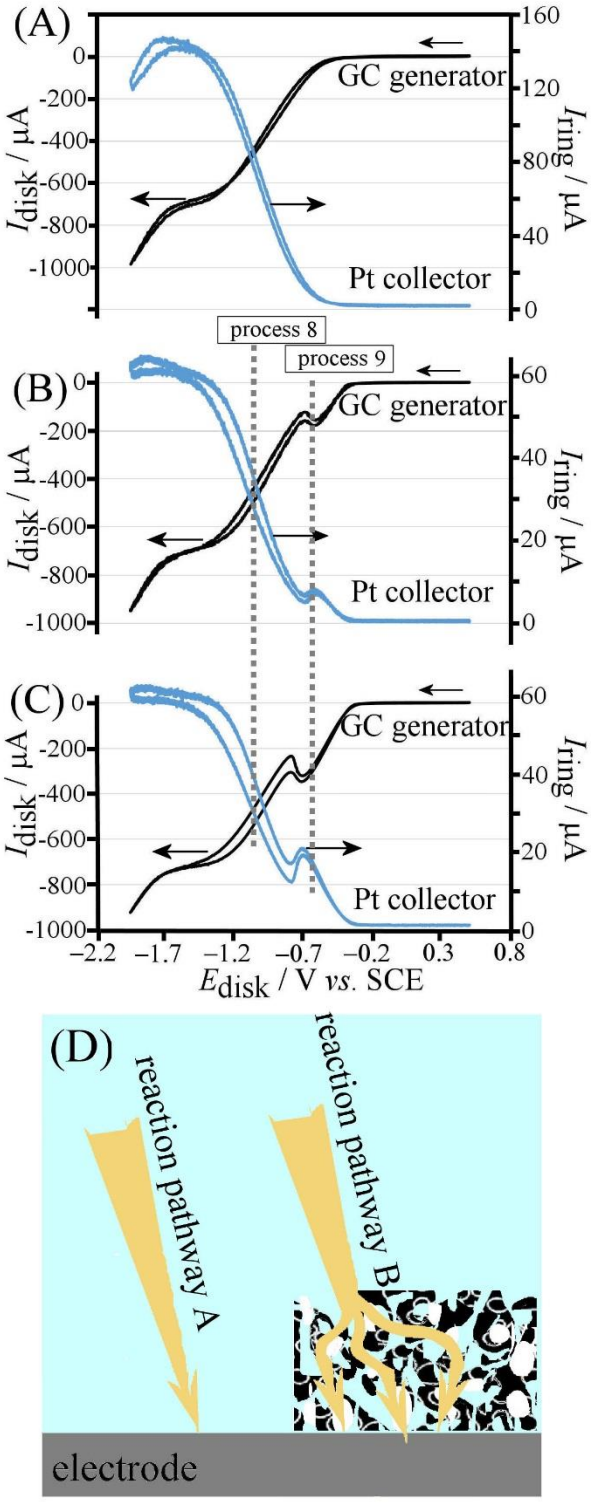

Figure 8. Cyclic voltammograms (scan rate 50 mVs^{-1}; rotating ring-disk electrode with a 5.5 mm diameter glassy carbon disc and a 2 mm wide platinum ring; 1500 rpm; ring potential +0.3 V vs. SCE) for the reduction of oxygen (1 bar oxygen purged solution) in 0.01 M phosphate buffer solution at pH 7 for (A) bare glassy carbon, (B) PIM-1 nanoparticle modified glassy carbon, and (C) PIM-PY nanoparticle modified glassy carbon. (D) Schematic drawing of reaction pathway A (Process 8; gas molecules diffuse from solution to the electrode surface) and reaction pathway B (Process 9; gas molecules accumulate in the intrinsically microporous polymer host and react at the electrode surface with apparently higher activity).

Data in Figure 8A show currents for processes in the absence of polymer coatings. The onset of oxygen reduction at glassy carbon occurs at approximately -0.6 V vs. SCE and the current then increases at more negative applied disk electrode potential to reach the mass transport limit at approximately -1.4 V vs. SCE. The simultaneously recorded anodic ring electrode current clearly shows that the main product in the oxygen reduction is hydrogen peroxide (equation 8). Only at more negative potential (with -1.7 V vs. SCE or more negative applied to the disk electrode) the production of hydrogen peroxide is lowered which is indicated by the loss of anodic current at the ring electrode.

When applying PIM-1 nanoparticles to the glassy carbon electrode (see Figure 8B) a new pre-peak is observed consistent with the reduction of oxygen that was stored in the polymer. The magnitude of the peak is not scan rate dependent but mass transport dependent. When decreasing the frequency of rotation of the ring-disk electrode to 1000 rpm or 100 rpm, the peak feature increases relative to the current plateau (not shown). Therefore the peak is associated with a pathway with oxygen either reacting *via* PIM (for low rates of mass transport) or directly at the glassy carbon electrode surface (for faster rates mass transport). At disk electrode potential more negative to this peak very similar characteristics and a mass transport limited plateau current essential identical to that observed in the absence of the polymer coating (see Figure 8A). The anodic ring current very closely follows the disk current and is therefore very likely to reflect the same mechanism (equation 8 and equation 9). The process in the pre-peak oxygen reduction produces hydrogen peroxide just as the main reduction process does. However, the magnitude of the anodic currents at the platinum ring electrode appears to be generally lower possibly due to some polymer nanoparticle coating affecting the access to the platinum ring surface. Both the plateau due to mass transport and the pre-peak feature appear to be steady state in nature as the peaks are clearly visible also when scanning the applied potential from negative to positive potentials. A similar experiment with PIM-PY nanoparticles (see Figure 8C) shows very similar features and therefore confirms that both PIMs give similar changes in behaviour during oxygen reduction.

Although it may seem tempting to assign observed effects of oxygen reduction catalysis at PIM polymer nanoparticle coated glassy carbon electrodes to a change in chemical environment, it is also possible to link the observed behaviour to the "triphasic" nature of the PIM materials. Figure 8D shows a schematic drawing of the glassy carbon surface with reaction pathway A describing processes at bare glassy carbon (Process 8) and reaction pathway B describing the processes in the potential range where the pre-peak is observed (Process 9). The rate of oxygen transport into the polymer must be linked to the switch from pathway A to B and to the magnitude of the peak current at -0.6 V vs. SCE.

The rate of the oxygen reduction (or the magnitude of the current) in the case of oxygen reduction on glassy carbon is dominated by kinetic control with a reversible potential for oxygen reduction at much more positive potentials. When expressing the rate of oxygen reduction as $rate = k_{het} \times [\text{oxygen}]$ (with k_{het} denoting a heterogeneous rate constant for electron transfer and assuming first order kinetics and [oxygen] denoting local oxygen concentration), there are three possible reasons for the rate to increase: (i) the rate constant can be affected by the chemical environment to give a faster (a chemical catalytic effect) process, or (ii) the local pH could be shifted to indirectly affect the rate constant via a shift in the equilibrium potential, or (iii) the apparent concentration of oxygen could be locally increased (a physical catalytic effect). The latter seems most likely in the PIM nanoparticle environment, since accumulation of gas (here oxygen) occurs. The release of this oxygen close to the location of the heterogeneous reaction can result in an apparently higher oxygen concentration due to the availability of oxygen from the triphasic system. The effects observed in this report suggest that the triphasic nature of the PIM materials can significantly affect redox process and thereby induce catalytic effects due to storage and accumulation of gas close to the electrode surface.

4. Summary and Conclusion

It has been shown that PIM-1 and PIM-PY materials when deposited as nanoparticulate or as continuous film at platinum or glassy carbon electrodes can substantially alter reaction pathways and electrocatalytic processes. Both polymers show similar voltammetric behaviour and for differences to be resolved in a more quantitative manner (or for quantitative comparison to a wider range of other microporous materials) further experiments will be required. Importantly, experiments are needed as a function of pH and of ionic strength. More work is

needed to further study the triphasic nature of these materials and to explore the effects this has on catalytic multi-phase processes at electrode surfaces. Better methods and theory are required to detect and monitor gas inclusions in PIMs *in situ* and to explore the effects of these inclusions on gas transport and reactivity. The chemical nature of these gas inclusions needs to be better understood. A wider range of gas redox reactions could be studied and notably the reduction of carbon dioxide could be investigated to see if it is beneficially affected simply based on the physical catalytic effects in addition to any chemical catalytic effects. Gas transport/mobility through PIM materials under triphasic conditions needs to be further investigated. A wider range of PIM materials could be developed and optimised for applications in triphasic electrocatalysis.

Acknowledgement

E.M. thanks the EPSRC (EP/K004956/1). F.M. and N.B.M. thank the Leverhulme Foundation (RPG-2014-308: "New Materials for Ionic Diodes and Ionic Photodiodes") for financial support.

References

[1] S. Shleev, V. Andoralov, D. Pankratov, M. Falk, O. Aleksejeva, Z. Blum, *Electroanalysis* **2016**, *28*, 2270–2287.

[2] S.Q. Lu, Z.B. Zhuang, *Sci. China Mater.* **2016**, *59*, 217–238.

[3] J. Gao, M.M. Zhu, H. Huang, Y. Liu, Z.H. Kang, *Inorg. Chem. Front.* **2017**, *4*, 1963–1986.

[4] K. Takanabe, *ACS Catal.* **2017**, *7*, 8006–8022.

[5] S. Anantharaj, S.R. Ede, K. Sakthikumar, K. Karthick, S. Mishra, S. Kundu, *ACS Catal.* **2016**, *6*, 8069–8097.

[6] C.A. Downes, S.C. Marinescu, *ChemSusChem* **2017**, *10*, 4374–4392.

[7] J.W. Zhou, B. Wang, *Chem. Soc. Rev.* **2017**, *46*, 6927–6945.

[8] K.L. Yeung, W. Han, *Catal. Today* **2014**, *236*, 182–205.

[9] S. Das, P. Heasman, T. Ben, S.L. Qiu, *Chem. Rev.* **2017**, *117*, 1515–1563.

[10] L. Borchardt, Q.L. Zhu, M.E. Casco, R. Berger, X.D. Zhuang, S. Kaskel, X.L. Feng, Q. Xu, *Mater. Today* **2017**, *20*, 592–610.

[11] N.B. McKeown, P.M. Budd, *Macromolecules* **2010**, *43*, 5163–5176.

[12] N.B. McKeown, *Sci. China Chem*. **2017**, *60*, 1023–1032.

[13] P.M. Budd, B.S. Ghanem, S. Makhseed, N.B. McKeown, K.J. Msayib, C.E. Tattershall, *Chem*. *Commun*. **2004**, 231–233.

[14] H.R. Kricheldorf, D. Fritsch, L. Vakhtangishvili, N. Lomadze, G. Schwarz, *Macromolecules* **2006**, *39*, 4990–4998.

[15] S. Kim, Y.M. Lee, *Prog. Polymer Sci.* **2015**, *43*, 1–32.

[16] R. Dawson, A.I. Cooper, D.J. Adams, *Polym*. *Internat*. **2013**, *62*, 345–352.

[17] D. Ramimoghadam, E.M. Gray, C.J. Webb, *Internat. J. Hydrogen Energy* **2016**, *41*, 16944–16965.

[18] Y. Wang, N.B. McKeown, K.J. Msayib, G.A. Turnbull, I.D.W. Samuel, *Sensors* **2011**, *11*, 2478–2487.

[19] E. Madrid, D.P. He, J.L. Yang, C.F. Hogan, B. Stringer, K.J. Msayib, N.B. McKeown, P.R. Raithby, F. Marken, *ChemElectroChem* **2016**, *3*, 2160–2164.

[20] S.E. Doris, A.L. Ward, P.D. Frischmann, L.J. Li, *J. Mater. Chem. A* **2016**, *4*, 16946–16952.

[21] F.J. Xia, M. Pan, S.C. Mu, R. Malpass-Evans, M. Carta, N.B. McKeown, G.A. Attard, A. Brew, D.J. Morgan, F. Marken, *Electrochim. Acta* **2014**, *128*, 3–9.

[22] Y.Y. Rong, A. Kolodziej, E. Madrid, M. Carta, R. Malpass-Evans, N.B. McKeown, F. Marken, *J. Electroanal. Chem*. **2016**, *779*, 241–249.

[23] Y.Y. Rong, Q.L. Song, K. Mathwig, E. Madrid, D.P. He, R.G. Niemann, P.J. Cameron, S.E.C. Dale, S. Bending, M. Carta, R. Malpass-Evans, N.B. McKeown, F. Marken, *Electrochem. Commun*. **2016**, *69*, 41–45.

[24] E. Madrid, Y.Y. Rong, M. Carta, N.B. McKeown, R. Malpass-Evans, G.A. Attard, T.J. Clarke, S.H. Taylor, Y.T. Long, F. Marken, *Angew. Chem. Int. Ed*. **2014**, *53*, 10751–10754.

[25] E. Madrid, P. Cottis, Y.Y. Rong, A.T. Rogers, J.M. Stone, R. Malpass-Evans, M. Carta, N.B. McKeown, F. Marken, *J. Mater. Chem. A* **2015**, *3*, 15849–15853.

[26] Y.Y. Rong, R. Malpass-Evans, M. Carta, N.B. McKeown, G.A. Attard, F. Marken, *Electroanalysis* **2014**, *26*, 904–909.

[27] D.P. He, Y.Y. Rong, M. Carta, R. Malpass-Evans, N.B. McKeown, F. Marken, *RSC Adv*. **2016**, *6*, 9315–9319.

[28] A.R. Langley, M. Carta, R. Malpass-Evans, N.B. McKeown, J.H.P. Dawes, E. Murphy, F. Marken, *Electrochim. Acta* **2018**, *260*, 348–357.

[29] Y.Y. Rong, D.P. He, A. Sanchez-Fernandez, C. Evans, K.J. Edler, R. Malpass-Evans, M. Carta, N.B. McKeown, T.J. Clarke, S.H. Taylor, A.J. Wain, J.M. Mitchels, F. Marken, *Langmuir* **2015**, *31*, 12300–12306.

[30] N. Hernandez, J. Iniesta, V.M. Leguey, R. Armstrong, S.H. Taylor, E. Madrid, Y.Y. Rong, R. Castaing, R. Malpass-Evans, M. Carta, N.B. McKeown, F. Marken, *Appl. Mater. Today* **2017**, *9*, 136–144.

[31] Y.Y. Rong, D.P, He, R. Malpass-Evans, M. Carta, N.B. McKeown, M.F. Gromboni, L.H. Mascaro, G.W. Nelson, J.S. Foord, P. Holdway, S.E.C. Dale, S. Bending, F. Marken, *Electrocatalysis* **2017**, *8*, 132–143.

[32] S.X. Leong, M. Carta, R. Malpass-Evans, N.B. McKeown, E. Madrid, F. Marken, *Electrochem. Commun.* **2018**, *86*, 17–20.

[33] R.R. Tiwari, J.Y. Jin, B.D. Freeman, D.R. Paul, *J. Membrane Sci.* **2017**, *537*, 362–371.

[34] B. Satilmis, P.M. Budd, *RSC Adv*. **2014**, *4*, 52189–52198.

[35] Q.L. Song, S. Cao, P. Zavala-Rivera, L.P. Lu, W. Li, Y. Ji, S.A. Al-Muhtaseb, A.K. Cheetham, E. Sivaniah, *Nature Commun.* **2013**, *4*, 1918.

[36] Q.L. Song, S. Cao, R.H. Pritchard, B. Ghalei, S.A. Al-Muhtaseb, E.M. Terentjev, A.K. Cheetham, E. Sivaniah, *Nature Commun.* **2014**, *5*, 4813.

[37] G.A. Gonzalez-Martinez, J.A. Zarate, A. Martinez, E. Sanchez-Gonzalez, J.R. Alvarez, E. Lima, E. Gonzalez-Zamora, I.A. Ibarra, *RSC Adv*. **2017**, *7*, 24833–24840.

[38] A.K. Kadoura, N. Nair, S. Sun, *Microporous Mesoporous Mater*. **2016**, *225*, 331–341.

[39] N.H. Linh, Y. Schuurman, D. Farrusseng, B. Coasne, *J. Phys. Chem. C* **2015**, *119*, 21547–21554.

[40] P. Billemont, B. Coasne, G. De Weireld, *Adsorption* **2014**, *20*, 453–463.

[41] J.T. Wang, S.F. Wang, Q.P. Xin, Y.F. Li, *J. Mater. Chem. A* **2017**, *5*, 6794–6816.

[42] N. Hernández-Ibáñez, J.S.M. Lee, J. Iniesta, V.M. Leguey, M.E. Briggs, A.I. Cooper, E. Madrid, F. Marken, *J. Electroanal. Chem*. **2017**, doi.org/10.1016/j.jelechem.2017.07.009.

[43] P.M. Budd, E.S. Elabas, B.S. Ghanem, S. Makhseed, N.B. McKeown, K.J. Msayib, C.E. Tattershall, D. Wang, *Adv. Mater.* **2004**, *16*, 456–459.

[44] J. Weber, A.J. Wain, G.A. Attard, F. Marken, *Electroanalysis* **2017**, *29*, 38–44.

[45] B.E. Conway, *Prog. Surface Sci.* **1995**, *49*, 331–452.

[46] J. Stacy, Y.N. Regmi, B. Leonard, M.H. Fan, *Renew. Sust. Energy Rev.* **2017**, *69*, 401–414.

[47] N.L. Pocard, D.C. Alsmeyer, R.L. Mccreery, T.X. Neenan, M.R. Callstrom, *J. Mater. Chem.* **1992**, *2*, 771–784.

[48] E.O. Barnes, G.E.M. Lewis, S.E.C. Dale, F. Marken, R.G. Compton, *Analyst* **2012**, *137*, 1068–1081.